doi:10.1038/nature13636

Migrations and dynamics of the intertropical convergence zone

Tapio Schneider[1,2], Tobias Bischoff[1,2] & Gerald H. Haug[2]

Rainfall on Earth is most intense in the intertropical convergence zone (ITCZ), a narrow belt of clouds centred on average around six degrees north of the Equator. The mean position of the ITCZ north of the Equator arises primarily because the Atlantic Ocean transports energy northward across the Equator, rendering the Northern Hemisphere warmer than the Southern Hemisphere. On seasonal and longer timescales, the ITCZ migrates, typically towards a warming hemisphere but with exceptions, such as during El Niño events. An emerging framework links the ITCZ to the atmospheric energy balance and may account for ITCZ variations on timescales from years to geological epochs.

The ITCZ can be identified as a tropical belt of deep convective clouds[1], or as the maximum in time-mean precipitation[2] (Fig. 1a). Seasonally, it migrates towards a hemisphere that warms relative to the other. Over the central Atlantic and Pacific oceans, the ITCZ migrates between 9° N in boreal summer and 2° N in boreal winter (Fig. 2a). Over the Indian Ocean and adjacent land surfaces, the ITCZ swings more dramatically between average latitudes of 20° N in boreal summer and 8° S in boreal winter, prompting the seasonal rainfall variations of the South Asian monsoon (Fig. 2b)[3]. On longer timescales, palaeo-records indicate that the ITCZ migrates similarly towards a differentially warming hemisphere[4,5]. For example, the boreal-summer ITCZ appears to have migrated southward as Northern Hemisphere summers cooled from the Holocene thermal maximum around 8,000 years before present (8 kyr BP) until the beginning of the Little Ice Age (LIA) at about 500 BP[6–8]. Simultaneously, summer monsoon rainfall in parts of South Asia weakened (Fig. 3a)[9–11], either because the ITCZ swung less far northward in boreal summer, or because its rainfall intensity weakened, or a combination of both[12,13]. These ITCZ variations over the Holocene arose because summer insolation in the Northern Hemisphere weakened with the precession of Earth's perihelion from Northern-Hemisphere towards Southern-Hemisphere summer[14,15]. But the annual-mean position of the ITCZ in the Northern Hemisphere (Fig. 1a) and the non-sinusoidal seasonal migrations in the South Asian monsoon sector (Fig. 2b)

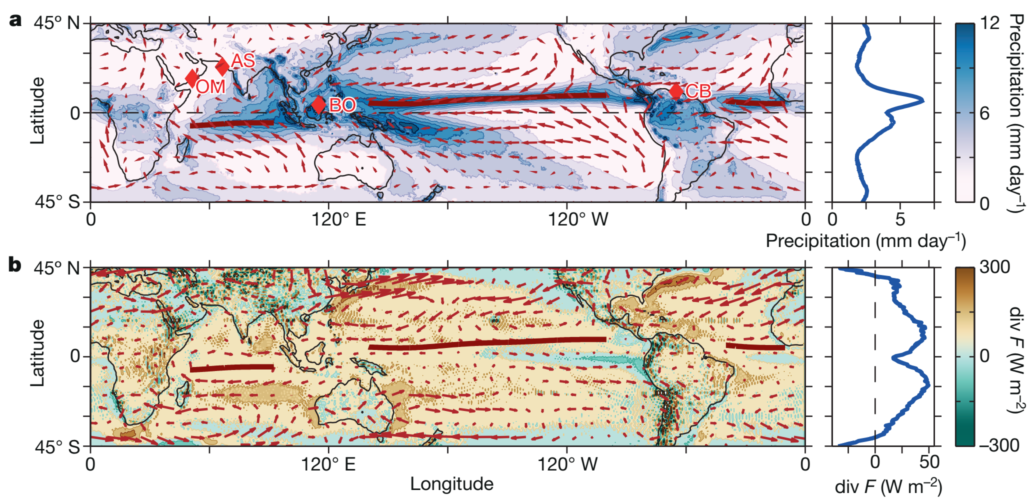

Figure 1 | Annual-mean precipitation, surface winds, and atmospheric energy balance. **a**, Precipitation (colour scale) is maximal at the ITCZ, and surface winds (vectors) converge there. The ITCZ over oceans (precipitation maxima) is marked by red lines. (Within the resolution of the data, convergence maxima of the surface winds and precipitation maxima coincide.) Other convergence zones, such as the South Pacific convergence zone, are also recognizable as precipitation maxima. The right panel shows the zonal-mean precipitation. The precipitation data are from the Tropical Rainfall Measuring Mission (TRMM) Multisatellite Precipitation Analysis (TMPA)[62] for 1998–2012. The wind data are from the European Centre for Medium-Range Weather Forecasts (ECMWF) interim reanalysis[44] for the same years. The longest wind vector (over the central Pacific) corresponds to a wind speed of 8.1 m s^{-1}. Also marked (red diamonds) are the sites of the palaeo-records shown in Figs 3 and 6: Oman (OM; 17° N, 51° E), Arabian Sea (AS; 23° N, 67° E), Borneo (BO; 4° N, 115° E), and the Cariaco basin (CB; 11° N, 65° W). **b**, Atmospheric moist static energy fluxes F (vectors) are weak near the ITCZ, but their divergence div F (colour scale) is generally positive there. (The ITCZ over oceans is marked by the same red lines as in **a**.) The right panel shows the zonal-mean divergence of the moist static energy flux. The energy flux data are from the ECMWF interim reanalysis for 1998–2012, corrected as in ref. 37 and provided by the National Center for Atmospheric Research. The longest vector (over the Kuroshio region) corresponds to a 2.7 × 10^{10} W m^{-1} energy flux.

[1]California Institute of Technology, Pasadena, California 91125, USA. [2]Department of Earth Sciences, ETH Zürich, 8092 Zürich, Switzerland.

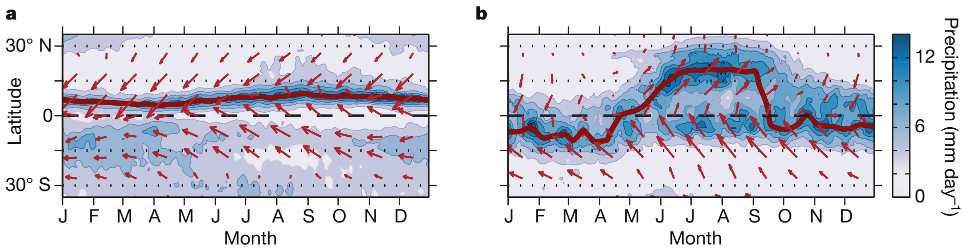

Figure 2 | Seasonal migration of the ITCZ over the Pacific and in the South Asian monsoon sector. Mean precipitation (colour scale) and surface winds (vectors) as a function of time of year averaged zonally over the Pacific (160° E–100° W) (**a**) and the South Asian monsoon sector (65° E–95° E) (**b**). (The annual cycle over the Atlantic is similar to that over the Pacific shown here, with slightly farther-southward (down to 2° N) excursions of the ITCZ in boreal winter.) The ITCZ (precipitation maxima) is marked by red lines. The seasonal ITCZ migration is sinusoidal with a moderate amplitude over the Pacific, away from continents; zonal winds remain easterly year-round (**a**). The seasonal ITCZ migration features abrupt and large shifts in the South Asian monsoon sector, marking the onset and retreat of the summer monsoon; zonal winds north of the Equator turn westerly at monsoon onset (**b**, see Box 1). The precipitation data are the daily TMPA data[62] averaged over 1998–2012. The data are smoothed temporally and meridionally by robust local linear regressions, spanning 11 days in time and 1° in latitude. The wind data are the 10-m winds from the ECMWF interim reanalysis[44] for the same years. The longest wind vector (in the South Asian monsoon sector at 18° S in September) corresponds to a wind speed of 9.1 m s^{-1}, and vector components to the left and right indicate westward and eastward wind components, respectively.

show that the ITCZ neither simply follows the insolation maximum[5,16–18], nor the sinusoidal seasonal variations of the interhemispheric temperature contrast. What mechanisms control the position of the ITCZ and its rainfall intensity is an important unanswered question in climate dynamics.

The ITCZ rainfall is fed by warm and moist trade winds near the surface (Figs 1a and 2). Their convergence leads to ascent of air masses, cooling, condensation and precipitation from deep convective clouds. In the upper troposphere, the air masses detrain from the clouds and diverge. They flow away from the ITCZ in the zonal mean, descend in the subtropics, and flow back along the surface towards the ITCZ, forming the meridionally overturning Hadley circulation (Fig. 4). The ITCZ must be understood as one facet of meridional overturning circulations and zonal overturning circulations such as the Walker circulation: as the location of their ascending branches. The ITCZ varies with the overturning circulations. The atmospheric circulations, in turn, interact with circulations in the underlying oceans, which modify the thermal conditions at the surface that drive the atmospheric circulations (Fig. 4).

Observations and simulations indicate that the ITCZ migrates meridionally and its rainfall intensity changes when the atmospheric energy balance shifts[19–32]. Elucidating how such ITCZ variations occur is the purpose

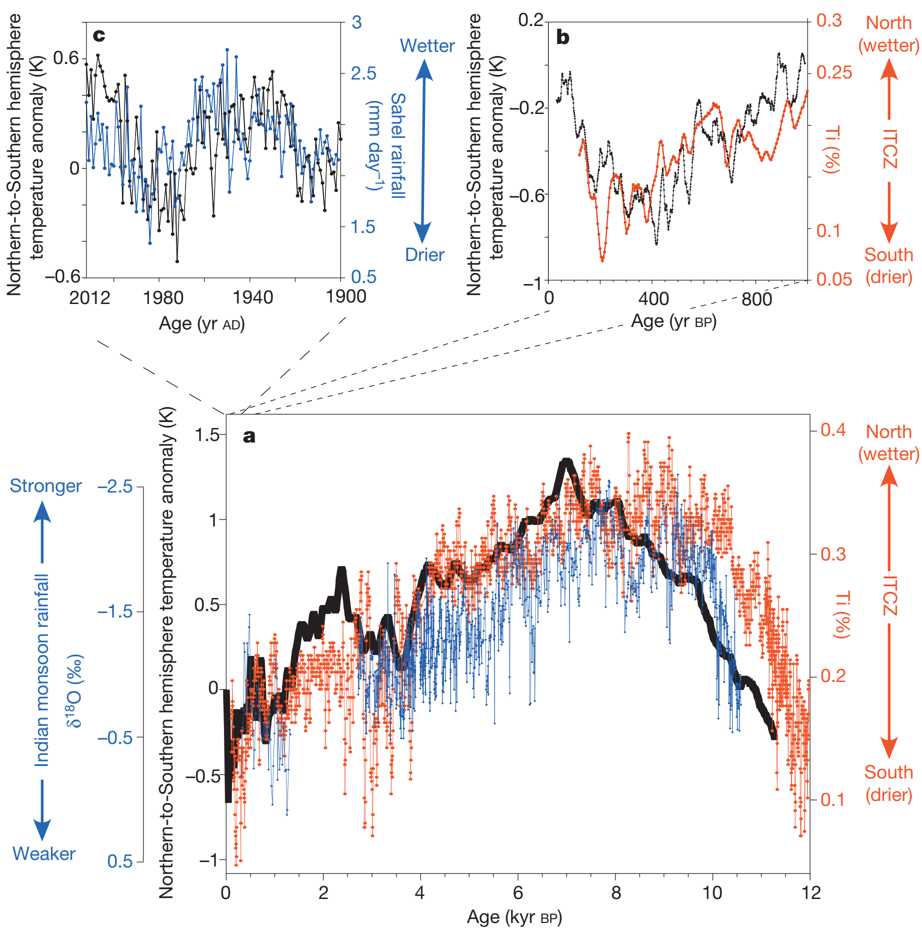

Figure 3 | Holocene ITCZ migrations, Indian monsoon and interhemispheric temperature contrast. **a**, Past 12,000 years. The temperature contrast between the extratropics of the Northern and Southern hemispheres (black) is strongly correlated with proxies of runoff into the Cariaco basin (red) and of Indian monsoon rainfall (blue). The temperature contrast is derived from the regularized expectation-maximization reconstructions in ref. 78, for areas poleward of 30° N and 30° S. The Cariaco runoff proxy is elemental titanium (Ti) in the ODP site 1002 sediment core (Fig. 1a), smoothed by a three-point running mean[7]. Higher Ti concentrations indicate more terrestrial runoff and rainfall, interpreted as a farther-northward ITCZ excursion in boreal summer[6,7]. Declining Ti concentrations indicate a southward migration of the boreal-summer ITCZ over the later Holocene. The Indian monsoon proxy is the abundance of oxygen-18 (δ^{18}O), relative to the Vienna Pee Dee Belemnite (VPDB) standard, in radiometrically dated cave stalagmites in Oman[9] (Fig. 1a). Increasing δ^{18}O values indicate weakening summer monsoon rainfall. **b**, Past 1,000 years. Ti in Cariaco sediments (red), with a higher-resolution reconstruction[98] of Northern Hemisphere temperatures (black, 20-point running mean). (Southern Hemisphere temperatures changed little during this time[83].) **c**, Past century. Temperature contrast between Northern and Southern hemisphere extratropics (poleward of 24° N and 24° S) based on instrumental data[60] (black), and average daily rainfall over the Sahel (12°–18° N, 20° W–35° E) during June–October based on land station data[99] (blue). All temperatures and temperature contrasts are given as anomalies relative to the 1960–91 AD mean.

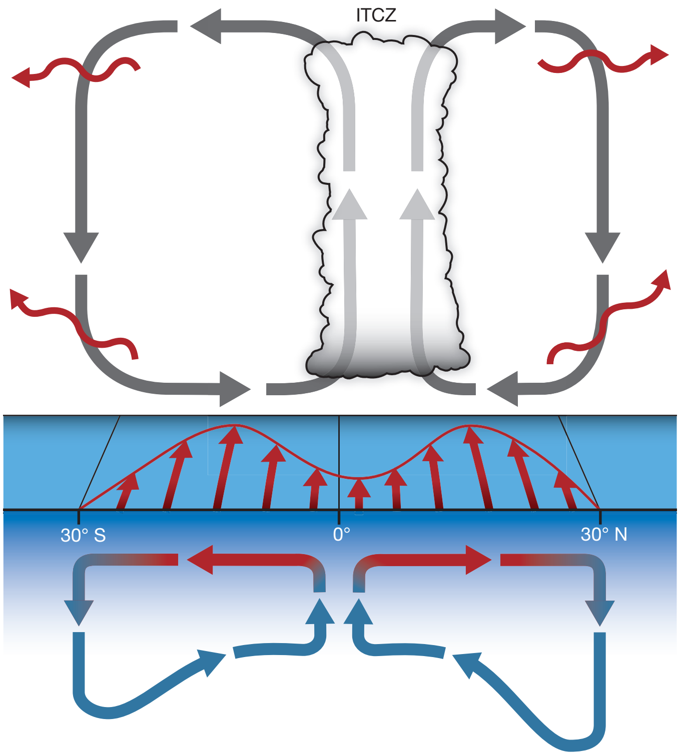

Figure 4 | Processes controlling zonal-mean ITCZ position. The lower branches of the Hadley circulation (grey arrows) bring warm and moist air masses towards the ITCZ, where they converge, rise and diverge as cooler and drier air masses aloft. Because the moist static energy aloft is greater than near the surface, the Hadley circulation transports energy away from the ITCZ. Eddies transport that energy farther into the extratropics (red wavy arrows). Hemispheric asymmetries in the energy export out of the tropics generally lead to an energy flux that crosses the Equator. Currently, the energy export into the extratropics in the south exceeds that in the north, leading to a southward cross-equatorial energy flux (Fig. 5). This implies an ITCZ in the Northern Hemisphere. Coupled to the Hadley circulation are mean zonal winds (red arrows at the sea surface), which are easterly where the near-surface mass flux is equatorward, and westerly where it is poleward. In the oceans, these zonal winds drive subtropical cells, with near-surface mass flux to the right of zonal winds in the Northern Hemisphere, and to the left in the Southern Hemisphere. Water masses cool and sink along their way towards the Hadley circulation termini and return below the sea surface (red and blue arrows). With mean easterlies in the tropics, the returning cool water masses upwell at the Equator, and the subtropical cells transport energy away from the Equator. But the upwelling location can migrate with the ITCZ away from the Equator and can dampen the ITCZ migration (Box 1).

of this Review. What emerges is a framework that links ITCZ variations to the energy input to and energy fluxes in the atmosphere. It allows us to interpret ITCZ variations across timescales from years to geological epochs.

Atmospheric energy balance and dynamics

Energy flux equator and ITCZ position

Although the air masses diverging in the upper troposphere above the ITCZ are cooler and drier than those converging near the surface, their potential energy is greater, such that their moist static energy—the energy relevant for transport considerations— is generally greater than that of the near-surface air masses[33,34]. Therefore, vertically integrated over atmospheric columns, deep overturning circulations such as the Hadley circulation transport energy in the direction of their upper branches: away from the ITCZ (Fig. 1b). Averaged over a span of longitudes wide enough that one can focus on meridional fluxes, the ITCZ can be expected to lie near the "energy flux equator"[21,22], where the atmospheric meridional energy flux F changes sign—insofar as eddy contributions to the tropical atmospheric energy flux divergence remain negligible[30,33]. Because the energy flux F usually increases going

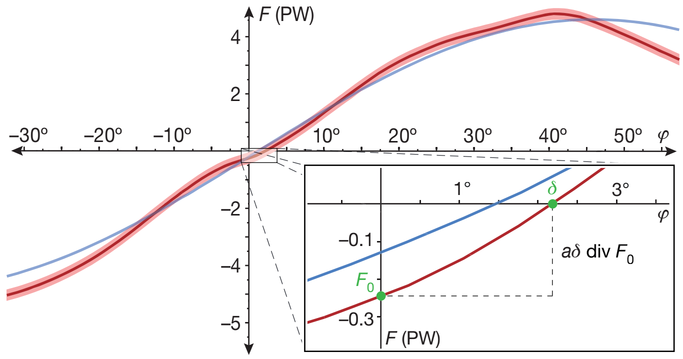

Figure 5 | Atmospheric meridional energy flux and energy flux equator. The atmospheric moist static energy flux F in the zonal and annual mean in the present climate (red line) is generally poleward, but it has a small southward component F_0 at the Equator. The energy flux equator is the zero of the energy flux, which currently lies around $\delta \approx 2.5°$. Given the equatorial values of the energy flux F_0 and of its 'slope' with latitude div F_0, the energy flux equator δ can be determined from $F_0 \approx -a\delta \operatorname{div} F_0$, where a is Earth's radius. For example, if F_0 increases (indicated schematically by the blue line), the energy flux equator δ moves southward. Similarly, if div F_0 increases, the energy flux equator moves towards the Equator. The energy flux data are from the ECMWF interim reanalysis for 1998–2012, corrected as in ref. 37 and provided by the National Center for Atmospheric Research. The light red shading indicates an estimated ±0.2 PW standard error (the actual uncertainty is poorly known).

northward in Earth's tropics—its divergence div F is usually positive, meaning that energy is exported out of the tropics (Fig. 1b)—one expects the energy flux equator and the ITCZ to lie farther north the stronger southward is the cross-equatorial energy flux F_0 (Fig. 5). This is indeed what is seen in observations and climate simulations[20–30,32]. Moreover, for a fixed cross-equatorial energy flux F_0, one expects the energy flux equator and the ITCZ to lie closer to the Equator for a steeper equatorial 'slope' div F of the energy flux with latitude (Fig. 5)[35].

More precisely, the atmospheric energy balance[33]

$$\operatorname{div} F = S - L - O \tag{1}$$

connects the divergence of the atmospheric energy flux F to the net energy input to the atmosphere, consisting of the net downward shortwave radiation S at the top of the atmosphere, minus the outgoing longwave radiation L and any ocean energy uptake O owing to transport or storage in the oceans. Energy storage on land is negligible on timescales of seasons and longer, as is storage in the atmosphere, at least in the tropics[36], on which we focus. Now we consider a zonal average over a span of longitudes (for example, an ocean basin) sufficiently wide that zonal fluxes can be ignored. By expanding the meridional energy flux F to first order in the latitude δ of the energy flux equator, we obtain $0 = F_\delta \approx F_0 + (\operatorname{div} F_0)a\delta$, where the subscripts δ and 0 indicate latitude, and a is Earth's radius (Fig. 5). Solving for the energy flux equator gives[35]

$$\delta \approx -\frac{1}{a}\frac{F_0}{S_0 - L_0 - O_0} \tag{2}$$

Hence, the energy flux equator, and approximately the ITCZ position, depend to first order on the cross-equatorial atmospheric energy flux F_0 and on the net energy input to the atmosphere at or near the Equator: $\operatorname{div} F_0 = S_0 - L_0 - O_0$. To be sure, the energy flux equator is not as sharply defined as is the ITCZ, because the nearly moist adiabatic thermal stratification implies that the atmospheric energy flux near the ITCZ is weak[34] (Fig. 1b). The energy flux equator also does not always coincide with the ITCZ (over the annual cycle[5,26] for example). But its meridional excursions have magnitudes similar to those of the ITCZ[5,22,35], so equation (2) provides a starting point for understanding the ITCZ position quantitatively.

In the present climate in the zonal and annual mean, the atmosphere transports 0.3 ± 0.2 PW of energy southward across the Equator (Fig. 5)[30,37]. The net equatorial energy input to the atmosphere[37] is 18 ± 3 W m^{-2} (Fig. 1b). With that, equation (2) implies an energy flux equator at 4° N ± 3°—broadly consistent with the actual energy flux equator (Fig. 5) and the mean ITCZ position[35]. However, the net equatorial energy input, $S_0 - L_0 - O_0$, is a small residual of large terms[37,38]: $S_0 \approx 323\ \mathrm{W\,m^{-2}}$, $L_0 \approx 251\ \mathrm{W\,m^{-2}}$ and $O_0 \approx 54\ \mathrm{W\,m^{-2}}$. Reducing S_0 or increasing L_0 or O_0 by only $6\ \mathrm{W\,m^{-2}}$ (by 2%–10%) suffices to move the energy flux equator δ a factor of about 1.5 farther poleward. The energy flux equator and ITCZ are sensitive to slight energetic shifts.

The mean position of the ITCZ in the Northern Hemisphere is thus linked to the atmospheric energy transport, which is directed from the warmer Northern Hemisphere into the 1.2–1.5 K cooler Southern Hemisphere[30,31,39]. The Northern Hemisphere is warmer primarily because the Atlantic's meridional overturning circulation (AMOC) transports energy northward, up the mean temperature gradient. It dominates the cross-equatorial ocean energy transport; the resulting net northward transport across the Equator amounts to about 0.5 PW in the zonal mean[30,37,39]. Some of this ocean energy transport across the Equator is compensated by the southward (downgradient) atmospheric energy transport, primarily accomplished by a Hadley cell with ascending branch and ITCZ north of the Equator (Fig. 4). (The Hadley cell, in turn, is often dominated by regional overturning cells, such as in the Asian monsoon sector[18].) The AMOC energy transport displaces the ITCZ north of the Equator also in the Pacific (Fig. 2a), because winds homogenize the effect of AMOC energy transport zonally in the extratropics; hence, the partially compensating atmospheric energy transport is more zonally uniform and affects the ITCZ similarly over the Atlantic and Pacific[32]. This global energetic perspective de-emphasizes atmosphere–ocean interactions triggered by the shape of coastlines, which had previously been suggested to control the mean ITCZ position[2,40]. Such local processes probably still play a role in shaping zonal asymmetries, but they appear to be secondary in displacing the Atlantic and Pacific ITCZ north of the Equator[28,30,31]. However, local processes do seem to be responsible for the annual-mean ITCZ position south of the Equator over the Indian Ocean (Fig. 1a). The southern ITCZ arises because in the Indian Ocean a secondary precipitation maximum is maintained south of the Equator even in boreal summer (Fig. 2b), probably because the northward monsoonal flow rises and generates precipitation south of the Equator[41], before crossing the Equator in the free troposphere and continuing towards the primary convergence zone farther north.

More generally, cross-equatorial atmospheric energy flux F_0 into one hemisphere demands an ITCZ in the opposite hemisphere, provided $\mathrm{div}\, F_0 > 0$. Equation (2) quantifies how much the ITCZ migrates northward when F_0 decreases (becomes more southward), and how much the ITCZ migrates equatorward when $S_0 - L_0 - O_0$ increases. Studies hitherto have focused on the cross-equatorial energy flux—or closely related meridional temperature gradients (see below). But the energy flux alone cannot determine the ITCZ position, because it has units of power rather than units of ITCZ displacement. The net equatorial energy input matters too. Often the two will vary simultaneously, so that the regression coefficient of the ITCZ position on F_0 alone, inferred in recent studies[24,26], generally differs from the corresponding coefficient in a bivariate regression on F_0 and $S_0 - L_0 - O_0$ (ref. 35). How the ITCZ globally and regionally depends on both should be analysed in simulations and observations.

However, equation (2) is merely an energy balance identity that does not in itself imply a direction of causality. To establish causal links, it is necessary to discuss how energetic shifts arise mechanistically.

Mechanisms of triggering ITCZ migrations

Simulations and records of past climates have established that hemispherically asymmetric changes in the extratropics—for example, in AMOC energy transport or ice cover—can trigger ITCZ migrations[5]. To explain how extratropical changes can shift the energy flux equator and ITCZ, we need to discuss a special property of tropical temperatures[21,23].

Tropical temperatures above the planetary boundary layer are dynamically constrained to vary only weakly in the horizontal[42] and to be nearly symmetric about the Equator. For example, in a Hadley circulation that is unaffected by eddy fluxes of angular momentum and that has an ITCZ far from the Equator, free-tropospheric temperatures are exactly symmetric about the Equator, despite the strong asymmetry of the circulation[43]. Indeed, hemispherically asymmetric variations of mid-tropospheric temperatures[44] currently do not exceed approximately 3 K in the zonal mean between 20° N and 20° S, not even in boreal summer, when strongly asymmetric monsoon circulations dominate the Hadley circulation.

The near-symmetry of tropical temperatures about the Equator means that a hemispherically asymmetric atmospheric energy export out of the tropics (say, across 30° N or 30° S) generally drives an energy flux across the Equator. To see this, assume that the tropics are confronted with a strengthening of the energy export across their northern boundary, which may be triggered by reduced AMOC energy transport or increased Arctic ice cover. First, we take cloud radiative effects and ocean energy uptake to be fixed, so that S and O stay fixed. In response to the perturbation at the northern boundary, temperatures may adjust throughout the tropics, but in the free troposphere they will remain nearly symmetric about the Equator—and so will the response of L, which depends on temperatures at the mid-tropospheric emission levels (for a fixed distribution of longwave absorbers and, in particular, clouds). Therefore, the response of $S - L - O$ is nearly symmetric about the Equator. The energy balance (equation (1)) then implies that the response of the energy flux F consists of a constant component F_0 and a component $F(\phi) \approx -F(-\phi)$ that is nearly antisymmetric about the Equator. The antisymmetric component is associated with hemispherically nearly symmetric energy export out of the tropics. So, to the extent that any hemispherically asymmetric energy export persists, it drives an energy flux F_0 through the tropics[35], leading to a northward cross-equatorial energy flux perturbation in our example. The energy flux equator (equation (2)), and with it the ITCZ, migrate southward.

Feedbacks from clouds, the distribution of water vapour, and ocean energy uptake modulate the ITCZ response, both by modulating $S_0 - L_0 - O_0$ and by inducing hemispheric asymmetries in the off-equatorial $S - L - O$ response, which modulate the F_0 response[35]. But because the longwave and shortwave effects of the deep ITCZ clouds nearly cancel[38,45], their feedback on the net radiative energy input $S - L$ is small. Other tropical cloud feedbacks may modulate $S - L$ further[22]. Yet their overall effect appears to be small; even its sign is uncertain[46]. The specific humidity of the atmosphere is enhanced near the ITCZ and reduces clear-sky L there. This, by itself, amplifies ITCZ migrations by increasing $S - L - O$ in the hemisphere with the ITCZ and amplifying the cross-equatorial energy flux into the opposite hemisphere. But because clear-sky variations in L near the ITCZ are only a small contributor to hemispheric asymmetries in L ($\leq 4\ \mathrm{W\,m^{-2}}$ in the annual mean according to satellite data[38]), this feedback is probably weak. Ocean energy uptake O may also cause hemispheric asymmetries in $S - L - O$. It and the shallow subtropical cells that dominate the ocean energy transport in low latitudes[47–49] interact with the ITCZ. When the ITCZ migrates sufficiently far from the Equator, upwelling of cold waters and ocean energy uptake is enhanced near the ITCZ and dampens the ITCZ migration (Box 1). In the Indian Ocean, this feedback dampens the seasonal ITCZ migrations of the South Asian monsoon[50,51]. It is probably even more important on longer timescales.

Thus, modulated by tropical feedbacks, hemispherically asymmetric energy export out of the tropics generally drives a cross-equatorial atmospheric energy flux. In the zonal and annual mean today, the atmosphere exports around 4 PW energy poleward across both 30° N and 30° S (Fig. 5), but it exports around 0.6 PW more southward than northward[31]. This in itself implies a southward atmospheric energy transport across the Equator of about 0.3 PW, consistent with the observed flux[30,37] $F_0 \approx -0.3 \pm 0.2$ PW. (A constant energy flux F_0 through the tropics adds to the energy export out of the tropics in one hemisphere and subtracts from it in the other, implying a hemispheric difference of $2F_0$ in energy exports.) Hemispheric asymmetries in $S - L - O$ within the tropics[35] contribute less to F_0. The southward cross-equatorial energy flux is extratropically triggered in that AMOC energy transport differentially reduces meridional temperature gradients in the northern extratropics. This weakens the energy export out of the northern tropics because it weakens the poleward eddy energy flux[30], which dominates the energy export[33] and generally strengthens both with increasing temperature gradients and temperatures (because specific humidities

BOX 1

Atmosphere–ocean coupling and feedback on ITCZ

Ekman balance, $fV = -\tau^x$ (where the Coriolis parameter is f, and the eastward surface stress is τ^x), holds outside the equatorial latitude belt between approximately 5° N and 5° S and links zonal surface winds to ageostrophic near-surface meridional mass fluxes in the atmosphere and oceans. The meridional Ekman mass flux V is directed to the right of the zonal surface stress τ^x in the Northern Hemisphere ($f > 0$), and to its left in the Southern Hemisphere ($f < 0$).

In the atmosphere, Ekman balance accounts for the near-surface mean meridional mass flux. The stress τ^x retards zonal surface winds u and thus has sign opposite to that of u. An equatorward near-surface flow ($fV < 0$) implies surface easterlies ($u < 0$). This is the case over the tropical Atlantic and Pacific year-round: the ITCZ does not migrate sufficiently far from the Equator to lead to poleward near-surface flow off the Equator (Fig. 2a). A poleward near-surface flow ($fV > 0$) off the Equator implies surface westerlies ($u > 0$), just as over the tropical Indian Ocean during the summer monsoon: the ITCZ migrates so far off the Equator that the zonal winds turn westerly (Fig. 2b).

In the oceans, Ekman balance accounts for most of the near-surface mean meridional mass flux in the shallow subtropical cells[47–49]. By Newton's third law, the wind stress τ^x driving V in the oceans is equal and opposite to the stress that retards the atmosphere's zonal winds over the oceans. Therefore, the near-surface Ekman mass flux is poleward ($fV > 0$) where zonal winds are easterly ($\tau^x < 0$), and equatorward otherwise. Remarkably, because the mean zonal stress on the atmosphere is equal and opposite to that on the oceans (up to the small surface stresses over land), the zonal-mean Ekman mass fluxes ($\pm\tau^x/f$) in the low-latitude atmosphere and oceans are approximately equal and opposite—even though water is a thousand times denser than air[49].

Thus the oceanic subtropical cells and the Hadley cells overhead resemble each other. Mirroring the upper branches of the Hadley cells, near-surface waters in the upper branches of the subtropical cells flow meridionally away from the ITCZ. They cool and are subducted on their way towards the Hadley circulation termini, where zonal surface winds turn westerly. The cooler water masses return below the surface and upwell near the ITCZ[47,48] (Fig. 4). This ocean circulation transports energy away from the upwelling region. Its zonal- and annual-mean energy transport is currently about as strong as the atmospheric energy transport[49], but it weakens as the climate warms[100]. Today, upwelling occurs at the Equator in the Atlantic and Pacific because mean zonal surface winds there are easterly year-round, so Ekman mass fluxes diverge at the Equator (f changes sign). But when the ITCZ is far enough from the Equator that tropical surface westerlies occur—such as in the Indian Ocean during the summer monsoon—upwelling occurs near the ITCZ, and the ocean can transport energy away from it. This increases the ocean energy uptake O and reduces the atmospheric energy input to the hemisphere with the ITCZ. It reduces the cross-equatorial atmospheric energy transport into the opposite hemisphere, thus dampening ITCZ migrations.

and latent energy fluxes increase with temperature)[35,52,53]. Ultimately, this chain of processes set in motion by AMOC energy transport leads to the mean position of the ITCZ north of the Equator[30,31]. Conversely, if AMOC energy transport were weaker or absent, the atmospheric energy export out of the tropics to the north may well exceed that to the south: the more prominent continentality of the Northern Hemisphere leads to stronger stationary eddies, which enhance the poleward eddy energy flux[33]. This may result in a northward F_0 and an ITCZ south of the Equator.

For the extratropical–tropical communication, then, it suffices to perturb the atmospheric energy export out of the tropics. Processes such as wind-induced evaporation, previously proposed as mediators between the extratropics and tropics[20], are not essential[25,32]. This energetic perspective is consistent with the notion that the ITCZ typically lies in the warmer hemisphere and migrates farther into that hemisphere the larger the interhemispheric temperature contrast[19–32]: Because tropical temperatures are nearly symmetric about the Equator, the warmer hemisphere will usually have weaker meridional temperature gradients in the extratropics, implying reduced energy export out of the tropics[52,53] and an ITCZ in that hemisphere. The larger the interhemispheric temperature contrast, the stronger is the unilateral reduction in energy export (other factors equal), and the farther in the warmer hemisphere is the ITCZ. Through closures for the atmospheric energy flux[23,24], the energy flux equator (equation (2)) and the ITCZ position have been quantitatively connected to temperatures, temperature gradients and other (for example, humidity) variables[35].

Towards a complete theory

The atmospheric energy balance is a starting point for understanding the ITCZ. But it gives an incomplete picture. The energy input to the atmosphere depends on the circulation, which must also satisfy other balances. In particular, the angular momentum balance is important for the Hadley circulation and convergence zones[53–57]. For example, the Hadley circulation undergoes a regime transition from an equinox regime, in which its angular momentum balance is dominated by eddy fluxes, to a monsoonal solstice regime, in which its angular momentum balance is less affected by eddy fluxes[18,55]. This regime transition is rendered abrupt by dynamical feedbacks within the Hadley circulation and in its interaction with extratropical eddies—feedbacks that may account for the square-wave shape of seasonal ITCZ migrations in the South Asian monsoon sector (Fig. 2b)[18]. In contrast, the energy flux equator migrates sinusoidally; it does not capture the ITCZ migrations fully[5]. For a full account, the energetic perspective must be paired with an account of the Hadley circulation—an outstanding challenge whose resolution may now be within reach because today's computational capabilities allow us to interrogate Hadley circulation dynamics systematically in experiments with global circulation models[53,56].

An account of the Hadley circulation is also necessary for a complete theory of how rainfall intensity in the ITCZ varies. Net precipitation (precipitation minus evaporation, measured, for example, by palaeo-proxies of continental runoff) is balanced by the convergence of water vapour in the atmosphere. Its variations consist of two components: a dynamic component associated with variations of the mass fluxes advecting the water vapour, and a thermodynamic component associated with variations of the specific humidity of the air masses[12]. The dynamic component includes migrations of the ITCZ and variations of Hadley circulation strength. Like the ITCZ position, the Hadley circulation strength depends on extratropical temperature gradients, among other factors, and so will also respond to extratropical changes[53,55]. Therefore, dynamic variations of ITCZ net precipitation can be expected to respond to Earth's orbital precession (which alters temperature gradients seasonally) and obliquity variations (which alter temperature gradients in the annual mean)[12,14], in addition to the response to variations in $S_0 - L_0 - O_0$. In contrast, thermodynamic variations of ITCZ net precipitation depend locally on the tropical energy balance, which controls the specific humidity[53]. The tropical energy balance in the annual mean is not affected by precession and is only weakly affected by obliquity variations[58]. But precession influences the specific humidity seasonally, and it can lead to an annual-mean thermodynamic rainfall response because seasonal humidity changes at a location are only relevant when the ITCZ is overhead, whereas annual-mean evaporation responses are weak[59]. A rich interplay of such dynamic and thermodynamic responses to different orbital variations probably caused the tropical rainfall variations indicated by palaeo-records.

Observations of ITCZ variations

Direct observations in the past century and palaeo-records for the more distant past afford instructive case studies of how the ITCZ varies with climate and how it shifts with the atmospheric energy balance.

Direct observations in the past century

El Niño and Southern Oscillation (ENSO). The alternation between warm El Niño and cold La Niña conditions in the eastern Pacific provides a counterexample to the notion that the ITCZ generally migrates towards a differentially warming hemisphere. Going from typical La Niña to El Niño conditions, annual-mean temperatures rise by around 0.1 K averaged globally, but the extratropics of the Northern Hemisphere warm 0.08 K more than those of the Southern Hemisphere (according to data from ref. 60). Yet the ITCZ shifts southward[61]. The shift is clearest in boreal winter: precipitation data[62] show that the western and central Pacific ITCZ shifts southward by about 2° going from typical La Niña to El Niño conditions, and by about 5° during strong El Niño events (such as in 1983 and 1998). Additionally, the longitudinal ITCZ structure is modified by ENSO's zonal rearrangement of convection[61].

The energy balance provides an explanation. Zonal-mean O_0 in boreal winter is approximately 15 W m^{-2} smaller during El Niño than during La Niña, with the largest changes in the eastern Pacific (according to the data described in refs 37 and 44; see also ref. 63). This reduction in ocean energy uptake increases $S_0 - L_0 - O_0$, which in the zonal mean in boreal winter more than doubles from typical La Niña to El Niño. It implies that the displacement of the energy flux equator (equation (2)) and of the ITCZ away from the Equator is reduced by more than a factor of two—sufficient to account for the observed shift in ITCZ position. The effect of changes in F_0 is smaller (about a quarter of the total shift). Thus, ENSO variations of the ITCZ position appear to be primarily driven by tropical changes in the atmospheric energy input.

Differential hemispheric warming. Increasing concentrations of greenhouse gases have led to global warming over the past century, which, however, was not uniform[27]. Until the 1930s, the northern extratropics warmed relative to the southern. Then, from the 1950s to the 1970s, the northern extratropics cooled by around 0.6 K relative to the southern extratropics. Since the mid-1970s, the northern extratropics have been warming again relative to the southern extratropics, thus far by around 0.7 K (Fig. 3c). (Differential warming rates for the entire hemispheres, rather than just the extratropics, are similar.) Differential warming of the northern extratropics is expected as concentrations of greenhouse gases increase: continents warm more than oceans and are more prominent in the Northern Hemisphere[64–66]. The differential cooling of the northern extratropics in the mid-twentieth century has been ascribed to increasing concentrations of anthropogenic aerosols in the Northern Hemisphere[67], and to natural variations particularly in the North Atlantic[68,69].

To the extent that tropical temperatures are symmetric about the Equator, warming of the northern relative to the southern extratropics differentially reduces meridional temperature gradients in the northern extratropics. This by itself should lead to differentially reduced eddy energy export out of the tropics into the Northern Hemisphere and a northward ITCZ migration. The converse holds for warming of the southern relative to the northern extratropics.

Tropical precipitation records are not accurate enough to assess past ITCZ migrations in detail. But there is evidence that the zonal-mean ITCZ migrated southward as the northern extratropics cooled differentially in the mid-twentieth century[70,71]; simulations show a similar response to increased anthropogenic aerosol loadings[70]. Consistently, the northward ITCZ excursion in boreal summer appears to have been capped at lower latitudes, at least over the Atlantic[72]. The neighbouring semi-arid African Sahel region, which lies at the northern limit of the seasonal ITCZ excursion over the continent, dried severely (Fig. 3c)[73–75]. Indeed, decadal variations of Sahel rainfall over the past century correlate with variations of the interhemispheric temperature contrast, including the differential warming of the northern extratropics (increasing Sahel rainfall) early in the twentieth century and since the 1980s (Fig. 3c).

Palaeo-records going back to the last ice age

Palaeoclimate data do not yet allow a global analysis of ITCZ variations but indicate globally coherent regional migrations. They suggest that the ITCZ position depends robustly on the interhemispheric temperature contrast, which—since the last ice age—has varied primarily because of: (1) Earth's precessional cycle[58], with a period of about 21 kyr; and (2) millennial climate changes around the North Atlantic, driven by changes in AMOC and glaciation[76,77].

Clear evidence for ITCZ migrations comes from the Cariaco basin[6,7] (Fig. 1a). There, the ITCZ during today's summers is overhead, trade winds and the ocean upwelling they drive are weak, and rainfall and runoff are at a maximum. Under such conditions, Cariaco sediments accumulate dark terrestrial detritus rich in elements such as titanium. In winter, the ITCZ migrates southward, trade winds and ocean upwelling strengthen, and runoff into the Cariaco basin is reduced. This increases the production of lightly coloured marine biogenic debris, which comes to dominate the flux to the sea bed[6]. From this alteration of Cariaco sediments, ITCZ migrations can be reconstructed.

Holocene. The Holocene (the past 11.7 kyr) represents the current interglacial (Fig. 3). Over its first 2–4 kyr, the Northern Hemisphere warmed[78] as glacial ice retreated[79]. But after the Holocene thermal maximum at around 8 kyr BP, one of the few remaining drivers of climate variations was the precessional cycle. Early in the Holocene, perihelion occurred during boreal summer, intensifying summer insolation in the Northern Hemisphere and weakening it in the Southern Hemisphere. Perihelion then precessed towards its current occurrence in boreal winter. At the Holocene thermal maximum at around 8 kyr BP, the boreal-summer insolation contrast between the northern and southern extratropics was 9% stronger than it is today[58]. The implied summertime warming of the northern extratropics relative to the southern should have led to a farther northward seasonal excursion of the ITCZ. (The excursion is modulated by equatorial insolation, which enters equation (2) through S_0 and was 5% stronger in boreal summer at 8 kyr BP; however, changes in S_0 are at least partially compensated by changes in L_0 and hence only represent a comparatively weak modulation of $S_0 - L_0 - O_0$.) Indeed, Cariaco sediments indicate greater summertime runoff around 8 kyr BP, followed by a gradual reduction until the beginning of the LIA at 500 BP (Fig. 3a, b). This signals a southward migration of the boreal-summer ITCZ, possibly paired with a thermodynamic reduction in rainfall intensity because of weakening local summer insolation. Cariaco runoff correlates well with reconstructions of the interhemispheric temperature contrast over the Holocene, which exhibits variations with amplitude (~0.6 K) similar to those seen over the past century (Fig. 3a,c)[7,78].

Consistent with the trend in the Cariaco record, the Atlantic ITCZ appears to have migrated southward over the Holocene[80]. Tropical West Africa dried[81] as the northern extratropics cooled differentially—the counterpart of the Sahel drying in the mid-twentieth century. The African Humid Period, during which lakes existed in the Sahara, appears to have terminated abruptly at around 5 kyr BP (ref. 81), perhaps when the boreal-summer ITCZ excursion over Africa ceased to reach the catchment areas of the sites from which the terminations are inferred. The complement to the reduction of boreal-summer rainfall in the northern tropics is a simultaneous increase of austral-summer rainfall in the southern tropics[4,82]. This indicates a precession-driven farther-southward excursion of the ITCZ in austral summer, prompted by an increasing south-to-north interhemispheric insolation contrast (3% greater in austral summer today than 8 kyr BP). But precession-driven thermodynamic rainfall changes may also play a part[59].

Superimposed on the Holocene trend in the Cariaco record are abrupt features that cannot be explained by orbital insolation changes. The most notable is reduced runoff into the Cariaco basin during the LIA (Fig. 3b). The LIA cooling appears to have been most pronounced in high northern latitudes; it is absent in much of the Southern Hemisphere[83]. Consistent with the implied differential cooling of the northern extratropics, Cariaco sediments suggest a southward ITCZ migration (Fig. 3b)[7]. Similarly, a variety of tropical Pacific records also indicate the ITCZ migrated southward during the LIA, followed by a northward migration at its end[84,85]. Thus, the LIA appears to elicit a southward ITCZ migration similar to the more gradual differential Holocene cooling of the Northern Hemisphere.

Last ice age. North Atlantic climate records from the last ice age are rife with millennial-scale climate variations, such as the Dansgaard–Oeschger cycles, in which rapid warming is followed by gradual cooling that often culminated in periods of massive iceberg discharge known as Heinrich stadials[76,86]. Variations in the Southern Hemisphere are less pronounced, so changes in the interhemispheric temperature contrast were dominated by high northern latitudes[87]. The origin of these cycles has eluded researchers for decades; AMOC changes are thought to play a role[88]. Whatever their origin, the ITCZ appears to have responded to the millennial variations in high northern latitudes in the same fashion as to the more recent changes in interhemispheric temperature contrast. Each time high northern latitudes cooled, a dry interval is observed in the Cariaco basin, signalling a southward ITCZ migration (Fig. 6a, b). Consistent with a southward ITCZ migration, increased rainfall is indicated in the southern tropics[4,89].

Rainfall reductions coeval with strong high-latitude coolings are also indicated by cave stalagmites from Borneo (Fig. 1a), where today's ITCZ passes overhead in boreal spring and fall (Fig. 6c)[90,91]. The fact that the Borneo record shows a response at least to the strongest millennial coolings in high latitudes suggests that it may likewise record ITCZ migrations. However, the slower orbital-timescale variations in the record correlate with local insolation when the ITCZ is overhead[90,91], suggesting that local thermodynamic rainfall variations may also play a part.

Monsoons and the ITCZ. Palaeo-records for the past 100 kyr indicate a strong correlation between the marine ITCZ position and monsoons[13]. Over the Holocene, as the boreal-summer position of the ITCZ migrated southward, Indian summer monsoon rainfall weakened[9,92] (Fig. 3a). During the last ice age and the millennial cold intervals in high northern latitudes, Indian monsoon rainfall dropped, to be reinvigorated during subsequent warm intervals (Fig. 6d)[11]. Cave stalagmites from eastern China[92,93] and a host of other hydroclimate reconstructions[94] exhibit similar changes over the Holocene and millennial variations during the last ice age. They also correlate with precession-driven changes in northern high-latitude summer insolation[93], which seasonally influences extratropical temperature gradients and the energy export out of the tropics.

The similarity of marine ITCZ and monsoon variations may be taken as evidence that monsoon variations indicate rainfall redistribution within the tropics and subtropics, with a northward displacement of the ITCZ implying increased rainfall farther north and decreased rainfall farther south[12,13]. However, thermodynamic rainfall variations prompted by precession-driven local insolation variations may also have a role[59]. The relative importance of dynamic and thermodynamic variations may shift with latitude and may account for the phase differences in rainfall variations seen, for example, between the Borneo and eastern China cave records[90,91].

Outlook

The energetic constraints on the ITCZ position have several implications. Stronger southward atmospheric energy transport across the Equator generally implies an ITCZ farther north; greater net energy input to the equatorial atmosphere implies an ITCZ closer to the Equator. The currently southward-directed cross-equatorial atmospheric energy transport weakens or reverses sign when the Northern Hemisphere extratropics cool relative to the southern extratropics, and this explains the southward ITCZ migrations that apparently occurred in the mid-twentieth century, LIA, and in cold intervals during the last ice age. Variations in the equatorial net energy input to the atmosphere modulate these ITCZ migrations, as they do during an El Niño. An outstanding challenge is to link orbital insolation variations to the shifts in the atmospheric energy balance that control the ITCZ position and its rainfall intensity—to arrive at a comprehensive understanding of tropical rainfall variations. Systematic studies with global climate models of how the tropical energy balance and extratropical energy fluxes respond to climate variations would be helpful. They will need to be accompanied by progress in our understanding of how clouds vary with climate and feed back onto the energy balance and ITCZ position.

The ITCZ position is sensitive to slight shifts in the atmospheric energy balance because the factors controlling it are small differences between large terms. The cross-equatorial energy flux depends on the small difference between the large energy exports out of the tropics into the northern and southern extratropics; the net energy input to the atmosphere is the small residual of the absorbed solar radiation, outgoing longwave radiation and

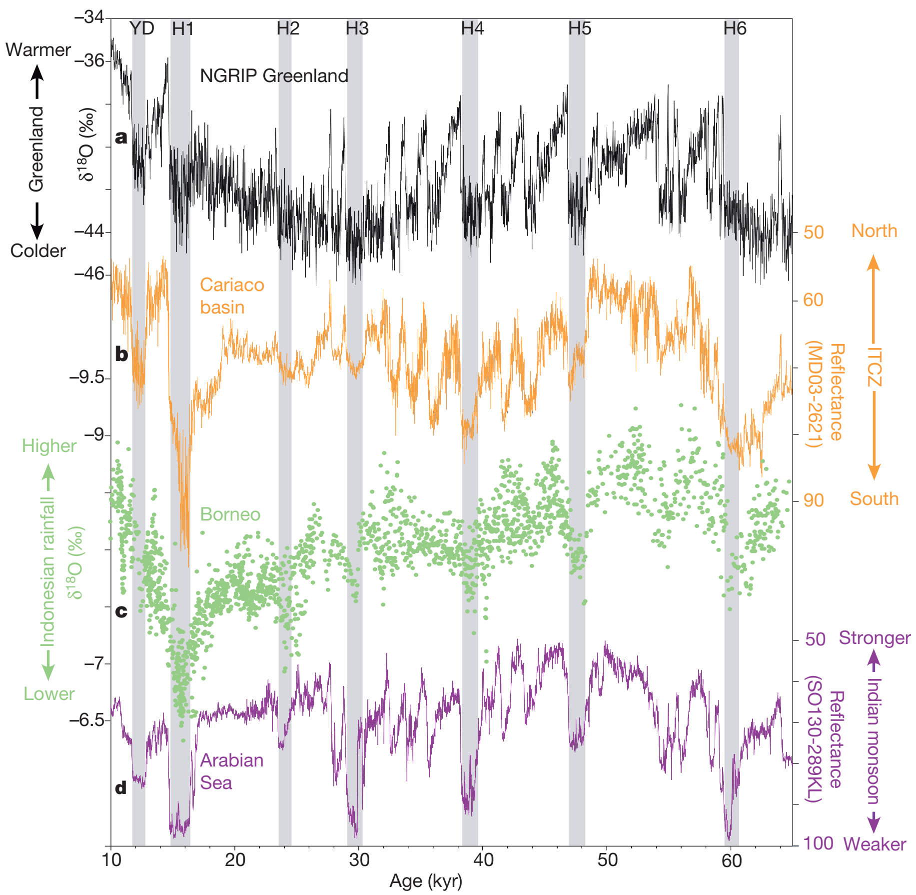

Figure 6 | Northern Hemisphere temperatures and ITCZ migrations during the last ice age. **a**, $\delta^{18}O$ from the North Greenland Ice Core Project (NGRIP) is a proxy of Arctic temperatures[86]. It indicates gradual warming after the Last Glacial Maximum (~20 kyr BP) and millennial-scale Dansgaard–Oeschger cycles, between cold (stadial) and warmer (interstadial) intervals[76]. Cold intervals include the Younger Dryas (YD) and Heinrich stadials H1 to H6 (grey shading). ($\delta^{18}O$ here is measured relative to Vienna Standard Mean Ocean Water (VSMOW).) **b**, Reflectance of Cariaco basin sediments measures the relative abundance of marine biogenic to terrigeneous deposits. It is high when rainfall and runoff are low[11]. Low reflectance is interpreted as a farther-northward ITCZ excursion in boreal summer. Warm intervals indicated by the Greenland ice core are generally associated with high runoff and a farther-northward boreal-summer ITCZ, and vice versa for cold intervals. During peak stadials, sediments lack the lamination produced by the annual rainfall cycle, indicating that the ITCZ appears to have been south of the Cariaco basin year-round[11]. **c**, $\delta^{18}O$, relative to the VPDB standard, in cave stalagmites from Borneo is a proxy of rainfall in the equatorial western Pacific[91]. It is low during Heinrich stadials, but Dansgaard–Oeschger cycles otherwise are less evident than in the higher-latitude records. **d**, Analogously to **b**, low reflectance of Arabian Sea sediments indicates high runoff from Indian monsoon rainfall[11]. It occurs during warm intervals indicated by the Greenland ice core. High reflectance and weaker Indian monsoon rainfall occur during cold intervals.

ocean energy uptake. Slight shifts in the large terms can lead to substantial ITCZ migrations. This sensitivity of the ITCZ position probably accounts for the difficulties climate models have in simulating it[95]. Biases in simulating the ITCZ can arise, for example, through relatively small errors in representing clouds: in the extratropics[29], they distort the energy export out of the tropics, and in the tropics[23], they distort the net energy input. Yet this sensitivity also makes the ITCZ an excellent recorder of how energetic balances shift with climate. Reconstructions of past ITCZ migrations may soon constrain predictions about the future in regions such as the Sahel, where slight modifications of seasonal ITCZ excursions can change the hydroclimate drastically[66]. As our theories advance and ITCZ and palaeoreconstructions improve, it may become possible to use inferences about how past ITCZ migrations depend on insolation variations to constrain uncertain cloud feedbacks. Particularly helpful would be reconstructions of the ITCZ in the mid-Pliocene (4.5–3.1 million years BP), the youngest geological analogue of a climate that is 2–3 K warmer. The Northern Hemisphere then was ice-free and relatively warm, suggesting a more northern ITCZ, while the equatorial eastern Pacific had a weaker cold tongue[96,97], suggesting reduced ocean energy uptake and an ITCZ closer to the Equator. Additionally, net energy input to the atmosphere was modified by increased concentrations of greenhouse gases[96] and cloud changes. Knowing how these competing effects balanced would reduce uncertainties in predictions for the next century.

Received 25 November 2013; accepted 1 July 2014.

1. Waliser, D. E. & Gautier, C. A satellite-derived climatology of the ITCZ. *J. Clim.* **6,** 2162–2174 (1993).
2. Philander, S. *et al.* Why the ITCZ is mostly north of the equator. *J. Clim.* **9,** 2958–2972 (1996).
3. Gadgil, S. The Indian monsoon and its variability. *Annu. Rev. Earth Planet. Sci.* **31,** 429–467 (2003).
4. Koutavas, A. & Lynch-Stieglitz, J. in *The Hadley Circulation: Present, Past, and Future* (eds Diaz, H. F. & Bradley, R. S.) Vol. 21 *Advances in Global Change Research* 347–369 (Kluwer Academic, 2004).
5. Chiang, J. C. H. & Friedman, A. R. Extratropical cooling, interhemispheric thermal gradients, and tropical climate change. *Annu. Rev. Earth Planet. Sci.* **40,** 383–412 (2012).
   This paper reviews evidence for the dependence of the ITCZ position on the interhemispheric temperature contrast.
6. Peterson, L. C., Haug, G. H., Hughen, K. A. & Rohl, U. Rapid changes in the hydrologic cycle of the tropical Atlantic during the last glacial. *Science* **290,** 1947–1951 (2000).
7. Haug, G. H., Hughen, K. A., Sigman, D. M., Peterson, L. C. & Röhl, U. Southward migration of the Intertropical Convergence Zone through the Holocene. *Science* **293,** 1304–1308 (2001).
8. Koutavas, A., deMenocal, P. B., Olive, G. C. & Lynch-Stieglitz, J. Mid-Holocene El Niño-Southern Oscillation (ENSO) attenuation revealed by individual foraminifera in eastern tropical Pacific sediments. *Geology* **34,** 993–996 (2006).
9. Fleitmann, D. *et al.* Holocene forcing of the Indian monsoon recorded in a stalagmite from southern Oman. *Science* **300,** 1737–1739 (2003).
10. Fleitmann, D. *et al.* Holocene ITCZ and Indian monsoon dynamics recorded in stalagmites from Oman and Yemen (Socotra). *Quat. Sci. Rev.* **26,** 170–188 (2007).
11. Deplazes, G. *et al.* Links between tropical rainfall and North Atlantic climate during the last glacial period. *Nature Geosci.* **6,** 213–217 (2013).
12. Clement, A. C., Hall, A. & Broccoli, A. J. The importance of precessional signals in the tropical climate. *Clim. Dyn.* **22,** 327–341 (2004).
13. Cheng, H., Sinha, A., Wang, X., Cruz, F. W. & Edwards, R. L. The global paleomonsoon as seen through speleothem records from Asia and the Americas. *Clim. Dyn.* **39,** 1045–1062 (2012).
14. Prell, W. L. & Kutzbach, J. E. Sensitivity of the Indian monsoon to forcing parameters and implications for its evolution. *Nature* **360,** 647–652 (1992).
15. Wanner, H. *et al.* Mid- to Late Holocene climate change: an overview. *Quat. Sci. Rev.* **27,** 1791–1828 (2008).
16. Chou, C. & Neelin, J. D. Mechanisms limiting the northward extent of the northern summer monsoons over North America, Asia, and Africa. *J. Clim.* **16,** 406–425 (2003).
17. Xian, P. & Miller, R. L. Abrupt seasonal migration of the ITCZ into the summer hemisphere. *J. Atmos. Sci.* **65,** 1878–1895 (2008).
18. Bordoni, S. & Schneider, T. Monsoons as eddy-mediated regime transitions of the tropical overturning circulation. *Nature Geosci.* **1,** 515–519 (2008).
19. Vellinga, M. & Wood, R. A. Global climatic impacts of a collapse of the Atlantic thermohaline circulation. *Clim. Change* **54,** 251–267 (2002).
20. Chiang, J. C. H. & Bitz, C. M. Influence of high latitude ice cover on the marine Intertropical Convergence Zone. *Clim. Dyn.* **25,** 477–496 (2005).
21. Broccoli, A. J., Dahl, K. A. & Stouffer, R. J. Response of the ITCZ to northern hemisphere cooling. *Geophys. Res. Lett.* **33,** L01702 (2006).
22. Kang, S. M., Held, I. M., Frierson, D. M. W. & Zhao, M. The response of the ITCZ to extratropical thermal forcing: idealized slab-ocean experiments with a GCM. *J. Clim.* **21,** 3521–3532 (2008).
23. Kang, S. M., Frierson, D. M. W. & Held, I. M. The tropical response to extratropical thermal forcing in an idealized GCM: The importance of radiative feedbacks and convective parameterization. *J. Atmos. Sci.* **66,** 2812–2827 (2009).
   This paper imposes cross-equatorial ocean energy transport in an idealized general circulation model and, following ref. 21, interprets ITCZ response through the atmosphere–ocean energy balance.
24. Frierson, D. M. W. & Hwang, Y.-T. Extratropical influence on ITCZ shifts in slab ocean simulations of global warming. *J. Clim.* **25,** 720–733 (2012).
25. Kang, S. M. & Held, I. M. Tropical precipitation, SSTs and the surface energy budget: a zonally symmetric perspective. *Clim. Dyn.* **38,** 1917–1924 (2012).
26. Donohoe, A., Marshall, J., Ferreira, D. & McGee, D. The relationship between ITCZ location and cross-equatorial atmospheric heat transport: from the seasonal cycle to the last glacial maximum. *J. Clim.* **26,** 3597–3618 (2013).
27. Friedman, A. R., Hwang, Y.-T., Chiang, J. C. H. & Frierson, D. M. W. Interhemispheric temperature asymmetry over the twentieth century and in future projections. *J. Clim.* **26,** 5419–5433 (2013).
28. Fučkar, N. S., Xie, S.-P., Farneti, R., Maroon, E. A. & Frierson, D. M. W. Influence of the extratropical ocean circulation on the Intertropical Convergence Zone in an idealized coupled general circulation model. *J. Clim.* **26,** 4612–4629 (2013).
29. Hwang, Y.-T. & Frierson, D. M. W. Link between the double-Intertropical Convergence Zone problem and cloud biases over the Southern Ocean. *Proc. Natl Acad. Sci. USA* **110,** 4935–4940 (2013).
30. Marshall, J., Donohoe, A., Ferreira, D. & McGee, D. The ocean's role in setting the mean position of the Inter-Tropical Convergence Zone. *Clim. Dyn.* **42,** 1967–1979 (2014).
   This paper shows that the northward AMOC energy transport is primarily responsible for the mean position of the ITCZ north of the Equator.
31. Frierson, D. M. W. *et al.* Contribution of ocean overturning circulation to tropical rainfall peak in the northern hemisphere. *Nature Geosci.* **6,** 940–944 (2013).
32. Kang, S. M., Held, I. M. & Xie, S.-P. Contrasting the tropical responses to zonally asymmetric extratropical and tropical thermal forcing. *Clim. Dyn.* **42,** 2033–2043 (2013).
33. Peixoto, J. P. & Oort, A. H. *Physics of Climate* (American Institute of Physics, 1992).
34. Neelin, J. D. & Held, I. M. Modeling tropical convergence based on the moist static energy budget. *Mon. Weath. Rev.* **115,** 3–12 (1987).
35. Bischoff, T. & Schneider, T. Energetic constraints on the position of the Intertropical Convergence Zone. *J. Clim.* **27,** 4937–4951 (2014).
36. Donohoe, A. & Battisti, D. S. The seasonal cycle of atmospheric heating and temperature. *J. Clim.* **26,** 4962–4980 (2013).
37. Fasullo, J. T. & Trenberth, K. E. The annual cycle of the energy budget. Part II: Meridional structures and poleward transports. *J. Clim.* **21,** 2313–2325 (2008).
38. Loeb, N. G. *et al.* Toward optimal closure of the Earth's top-of-atmosphere radiation budget. *J. Clim.* **22,** 748–766 (2009).
39. Feulner, G., Rahmstorf, S., Levermann, A. & Volkwardt, S. On the origin of the surface air temperature difference between the hemispheres in Earth's present-day climate. *J. Clim.* **26,** 7136–7150 (2013).
40. Xie, S.-P. in *The Hadley Circulation: Present, Past and Future* (eds Diaz, H. F. & Bradley, R. S.) Vol. 21 *Advances in Global Change Research* 121–152 (Kluwer Academic, 2004).
   This paper reviews how the shape of continents and atmosphere–ocean interactions can cause zonal asymmetries and displace the ITCZ north of the Equator.
41. Pauluis, O. Boundary layer dynamics and cross-equatorial Hadley circulation. *J. Atmos. Sci.* **61,** 1161–1173 (2004).
42. Charney, J. G. A note on large-scale motions in the tropics. *J. Atmos. Sci.* **20,** 607–609 (1963).
43. Lindzen, R. S. & Hou, A. Y. Hadley circulations for zonally averaged heating centered off the equator. *J. Atmos. Sci.* **45,** 2416–2427 (1988).
44. Dee, D. P. *et al.* The ERA-Interim reanalysis: configuration and performance of the data assimilation system. *Q. J. R. Meteorol. Soc.* **137,** 553–597 (2011).
45. Harrison, E. F. *et al.* Seasonal variation of cloud radiative forcing derived from the Earth Radiation Budget Experiment. *J. Geophys. Res.* **95,** 18687–18703 (1990).
46. Voigt, A., Stevens, B., Bader, J. & Mauritsen, T. Compensation of hemispheric albedo asymmetries by shifts of the ITCZ and tropical clouds. *J. Clim.* **27,** 1029–1045 (2014).
47. Schott, F. A., McCreary, J. P. Jr & Johnson, G. C. in *Earth's Climate: The Ocean-Atmosphere Interaction* Geophysical Monograph Series 147, 261–304 (American Geophysical Union, 2004).
48. Klinger, B. A. & Marotzke, J. Meridional heat transport by the subtropical cell. *J. Phys. Oceanogr.* **30,** 696–705 (2000).
49. Held, I. M. The partitioning of the poleward energy transport between the tropical ocean and atmosphere. *J. Atmos. Sci.* **58,** 943–948 (2001).
50. Jayne, S. R. & Marotzke, J. The dynamics of ocean heat transport variability. *Rev. Geophys.* **39,** 385–411 (2001).
51. Webster, P. J. in *The Asian Monsoon* (ed. Wang, B.) 3–66 (Springer Praxis, 2006).
52. Caballero, R. & Langen, P. L. The dynamic range of poleward energy transport in an atmospheric general circulation model. *Geophys. Res. Lett.* **32,** L02705 (2005).
53. Schneider, T., O'Gorman, P. A. & Levine, X. J. Water vapor and the dynamics of climate changes. *Rev. Geophys.* **48,** RG3001 (2010).
   This paper reviews how the hydrological cycle, the Hadley circulation, and extratropical energy transports vary with climate.
54. Held, I. M. & Hou, A. Y. Nonlinear axially symmetric circulations in a nearly inviscid atmosphere. *J. Atmos. Sci.* **37,** 515–533 (1980).

55. Walker, C. C. & Schneider, T. Eddy influences on Hadley circulations: simulations with an idealized GCM. *J. Atmos. Sci.* **63,** 3333–3350 (2006).
56. Schneider, T. The general circulation of the atmosphere. *Annu. Rev. Earth Planet. Sci.* **34,** 655–688 (2006).
57. Schneider, T. & Bordoni, S. Eddy-mediated regime transitions in the seasonal cycle of a Hadley circulation and implications for monsoon dynamics. *J. Atmos. Sci.* **65,** 915–934 (2008).
58. Berger, A. & Loutre, M. F. Insolation values for the climate of the last 10 million years. *Quat. Sci. Rev.* **10,** 297–317 (1991).
59. Merlis, T. M., Schneider, T., Bordoni, S. & Eisenman, I. The tropical precipitation response to orbital precession. *J. Clim.* **26,** 2010–2021 (2013).
60. Hansen, J., Ruedy, R., Sato, M. & Lo, K. Global surface temperature change. *Rev. Geophys.* **48,** RG4004 (2010).
61. Dai, A. & Wigley, T. M. L. Global patterns of ENSO-induced precipitation. *Geophys. Res. Lett.* **27,** 1283–1286 (2000).
62. Liu, Z., Ostrenga, D., Teng, W. & Kempler, S. Tropical Rainfall Measuring Mission (TRMM) precipitation data and services for research and applications. *Bull. Am. Meteorol. Soc.* **93,** 1317–1325 (2012).
63. Trenberth, K. E., Caron, J. M., Stepaniak, D. P. & Worley, S. Evolution of El Niño-Southern Oscillation and global atmospheric surface temperatures. *J. Geophys. Res.* **107,** 4065, http://dx.doi.org/10.1029/2000JD000298 (2002).
64. Joshi, M. M., Gregory, J. M., Webb, M. J., Sexton, D. M. H. & Johns, T. C. Mechanisms for the land/sea warming contrast exhibited by simulations of climate change. *Clim. Dyn.* **30,** 455–465 (2008).
65. Byrne, M. P. & O'Gorman, P. A. Link between land-ocean warming contrast and surface relative humidities in simulations with coupled climate models. *Geophys. Res. Lett.* **40,** 5223–5227 (2013).
66. Broecker, W. S. & Putnam, A. E. Hydrologic impacts of past shifts of Earth's thermal equator offer insight into those to be produced by fossil fuel CO_2. *Proc. Natl Acad. Sci. USA* **110,** 16710–16715 (2013).
67. Tett, S. F. B. *et al.* Estimation of natural and anthropogenic contributions to twentieth century temperature change. *J. Geophys. Res.* **107,** 4306 http://dx.doi.org/10.1029/2000JD000028 (2002).
68. Schneider, T. & Held, I. M. Discriminants of twentieth-century changes in Earth surface temperatures. *J. Clim.* **14,** 249–254 (2001).
69. Thompson, D. W. J., Wallace, J. M., Kennedy, J. J. & Jones, P. D. An abrupt drop in northern hemisphere sea surface temperature around 1970. *Nature* **467,** 444–447 (2010).
70. Rotstayn, L. D. & Lohmann, U. Tropical rainfall trends and the indirect aerosol effect. *J. Clim.* **15,** 2103–2116 (2002).
This paper demonstrates that increased atmospheric aerosol loading can lead to southward ITCZ migrations and presents evidence that this occurred in the twentieth century.
71. Hwang, Y.-T., Frierson, D. M. W. & Kang, S. M. Anthropogenic sulfate aerosol and the southward shift of tropical precipitation in the late 20th century. *Geophys. Res. Lett.* **40,** 2845–2850 (2013).
72. Tokinaga, H. & Xie, S.-P. Weakening of the equatorial Atlantic cold tongue over the past six decades. *Nature Geosci.* **4,** 222–226 (2011).
73. Folland, C. K., Palmer, T. N. & Parker, D. E. Sahel rainfall and worldwide sea temperatures, 1901–85. *Nature* **320,** 602–607 (1986).
74. Giannini, A., Saravanan, R. & Chang, P. Oceanic forcing of Sahel rainfall on interannual to interdecadal time scales. *Science* **302,** 1027–1030 (2003).
75. Held, I. M., Delworth, T. L., Lu, J., Findell, K. L. & Knutson, T. R. Simulation of Sahel drought in the 20th and 21st centuries. *Proc. Natl Acad. Sci. USA* **102,** 17891–17896 (2005).
This paper presents an overview of the mid-20th century Sahel drought, including its causes and predictions for the future.
76. Bond, G. *et al.* Correlations between climate records from North Atlantic sediments and Greenland ice. *Nature* **365,** 143–147 (1993).
77. Broecker, W. Massive iceberg discharges as triggers for global climate change. *Nature* **372,** 421–424 (1994).
78. Marcott, S. A., Shakun, J. D., Clark, P. U. & Mix, A. C. A reconstruction of regional and global temperature for the past 11,300 years. *Science* **339,** 1198–1201 (2013).
79. Renssen, H. *et al.* The spatial and temporal complexity of the Holocene thermal maximum. *Nature Geosci.* **2,** 411–414 (2009).
80. Arbuszewski, J. A., deMenocal, P. B., Cléroux, C., Bradtmiller, L. & Mix, A. Meridional shifts of the Atlantic intertropical convergence zone since the Last Glacial Maximum. *Nature Geosci.* **6,** 959–962 (2013).
This paper infers ITCZ migrations from reconstructions of ocean salinity, which diversifies evidence for ITCZ migrations and may eventually allow reconstructions of rainfall at the ITCZ.
81. deMenocal, P. *et al.* Abrupt onset and termination of the African Humid Period: rapid climate responses to gradual insolation forcing. *Quat. Sci. Rev.* **19,** 347–361 (2000).
82. Baker, P. A. *et al.* Tropical climate changes at millennial and orbital timescales on the Bolivian Altiplano. *Nature* **409,** 698–701 (2001).
83. Jones, P. D., Briffa, K. R., Barnett, T. P. & Tett, S. F. B. High-resolution palaeoclimatic records for the last millennium: interpretation, integration and comparison with general circulation model control-run temperatures. *Holocene* **8,** 455–471 (1998).
84. Linsley, B. K., Dunbar, R. B., Wellington, G. M. & Mucciarone, D. A. A coral-based reconstruction of Intertropical Convergence Zone variability over Central America since 1707. *J. Geophys. Res.* **99,** 9977–9994 (1994).
85. Sachs, J. P. *et al.* Southward movement of the Pacific Intertropical Convergence Zone AD 1400–1850. *Nature Geosci.* **2,** 519–525 (2009).
This paper presents evidence that the ITCZ across the Pacific was farther south during the Little Ice Age.
86. Wolff, E. W., Chappellaz, J., Blunier, T., Rasmussen, S. O. & Svensson, A. Millennial-scale variability during the last glacial: The ice core record. *Quat. Sci. Rev.* **29,** 2828–2838 (2010).
87. Blunier, T. *et al.* Asynchrony of Antarctic and Greenland climate change during the last glacial period. *Nature* **394,** 739–743 (1998).
88. Broecker, W. S. Thermohaline circulation, the Achilles heel of our climate system: Will man-made CO_2 upset the current balance? *Science* **278,** 1582–1588 (1997).
89. Wang, X. *et al.* Wet periods in northeastern Brazil over the past 210 kyr linked to distant climate anomalies. *Nature* **432,** 740–743 (2004).
90. Partin, J. W., Cobb, K. M., Adkins, J. F., Clark, B. & Fernandez, D. P. Millennial-scale trends in west Pacific warm pool hydrology since the Last Glacial Maximum. *Nature* **449,** 452–455 (2007).
91. Carolin, S. A. *et al.* Varied response of western Pacific hydrology to climate forcings over the last glacial period. *Science* **340,** 1564–1566 (2013).
92. Wang, Y. *et al.* The Holocene Asian monsoon: links to solar changes and North Atlantic climate. *Science* **308,** 854–857 (2005).
This paper shows that Asian monsoon rainfall weakened over the past 8 kyr.
93. Wang, Y. *et al.* Millennial-and orbital-scale changes in the East Asian monsoon over the past 224,000 years. *Nature* **451,** 1090–1093 (2008).
94. An, Z. S. The history and variability of the East Asian paleomonsoon climate. *Quat. Sci. Rev.* **19,** 171–187 (2000).
95. Lin, J.-L. The double-ITCZ problem in IPCC AR4 coupled GCMs: ocean–atmosphere feedback analysis. *J. Clim.* **20,** 4497–4525 (2007).
96. Fedorov, A. V. *et al.* Patterns and mechanisms of early Pliocene warmth. *Nature* **496,** 43–49 (2013).
97. Zhang, Y. G., Pagani, M. & Liu, Z. A 12-million-year temperature history of the tropical Pacific Ocean. *Science* **344,** 84–87 (2014).
98. Moberg, A., Sonechkin, D. M., Holmgren, K., Datsenko, N. M. & Karlén, W. Highly variable northern hemisphere temperatures reconstructed from low- and high-resolution proxy data. *Nature* **433,** 613–617 (2005).
99. Harris, I., Jones, P. D., Osborn, T. J. & Lister, D. H. Updated high-resolution grids of monthly climatic observations—the CRU TS3.10 dataset. *Int. J. Climatol.* **34,** 623–642 (2014).
100. Levine, X. J. & Schneider, T. Response of the Hadley circulation to climate change in an aquaplanet GCM coupled to a simple representation of ocean heat transport. *J. Atmos. Sci.* **68,** 769–783 (2011).

Acknowledgements J. Fasullo and K. Trenberth from the National Center for Atmospheric Research provided the energy flux data we used in Figs 1b and 5 and in some of the estimates in the text. The top-of-atmosphere radiative flux estimates in the text are based on NASA Clouds and the Earth's Radiant Energy System (CERES) data, version CERES EBAF-TOA Ed2.7. S. Marcott provided the temperature reconstructions in Fig. 3, and M. Hell drew Figs 4 and 5. We are grateful for discussions with D. Sigman and N. Meckler and for comments on drafts by F. Ait-Chaalal, A. Donohoe, R. Ferrari, and J.-E. Lee. The research underlying this paper was supported by grants from the US National Science Foundation (numbers AGS-1019211, AGS-1049201 and AGS-1003614).

Author Contributions All authors discussed the central concepts and ideas and processed and analysed data. T.S. and G.H.H. led the writing of the paper.

Author Information Reprints and permissions information is available at www.nature.com/reprints. The authors declare no competing financial interests. Readers are welcome to comment on the online version of the paper. Correspondence should be addressed to T.S. (tapio@ethz.ch).